Journal of Anatomy

J. Anat. (2008) **213**, pp509–519 doi: 10.1111/j.1469-7580.2008.00970.x

Microcephalia with mandibular and dental dysplasia in adult Zmpste24-deficient mice

F. de Carlos,[1,4] I. Varela,[2,5] A. Germanà,[6] G. Montalbano,[6] J. M. P. Freije,[2,5] J. A. Vega,[3] C. López-Otin[2,5] and J. M. Cobo[1,4]

[1]*Departamentos de Cirugía y Especialidades Médico-Quirúrgicas (Area de Estomatología),* [2]*Bioquímica y Biología Molecular, and* [3]*Morfología y Biología Celular, Universidad de Oviedo, Spain*
[4]*Instituto Asturiano de Odontología, Oviedo, Spain*
[5]*Instituto Universitario de Oncología, Universidad de Oviedo, Spain*
[6]*Dipartimento di Morfologia, Biochimica, Fisiologia e Produzione Animale (Sezione di Morfologia), Università di Messina, Italy*

Abstract

ZMPSTE24 (also called FACE-1) is a zinc-metalloprotease involved in the post-translational processing of prelamin A to mature lamin A, a major component of the nuclear envelope. Mutations in the *ZMPSTE24* gene or in that encoding its substrate prelamin A (*LMNA*) result in a series of human inherited diseases known collectively as laminopathies and showing regional or systemic manifestations (i.e. the Hutchinson–Gilford progeria syndrome). Typically, patients suffering some laminopathies show craniofacial or mandible anomalies, aberrant dentition or facial features characteristic of aged persons. To analyse whether *Zmpste24*$^{-/-}$ mice reproduce the cranial phenotype observed in humans due to mutations in *ZMPSTE24* or *LMNA*, we conducted a craniometric study based on micro-computer tomography (μCT) images. Furthermore, using simple radiology, μCT, μCT-densitometry and scanning electron microscopy, we analysed the mandible and the teeth from *Zmpste24*$^{-/-}$ mice. Finally, the structure of the lower incisor was investigated using an H&E technique. The results demonstrate that *Zmpste24*$^{-/-}$ mice are microcephalic and show mandibular and dental dysplasia affecting only the mandible teeth. In all cases, the lower incisor of mice lacking *Zmpste24* was smaller than in control animals, showed cylindrical morphology and a transverse fissure at the incisal edge, and the pulpal cavity was severely reduced. Structurally, the dental layers were normally arranged but cellular layers were disorganized. The inferior molars showed a reduced cusp size. Taken together, these data strongly suggest that *Zmpste24*$^{-/-}$ mice represent a good model to analyse the craniofacial and teeth malformations characteristic of lamin-related pathologies, and might contribute to a better understanding of the molecular events underlying these diseases.

Key words cephalometry; metalloproteinase; micro-CT; nuclear envelope; progeroid syndromes; tooth.

Introduction

The lamins are type-V intermediate filaments arranged as a network forming the nuclear lamina, a structure adjacent and attached to the inner nuclear membrane through interactions with integral membrane proteins (Mounkes & Stewart, 2004; Worman & Courvalin, 2005; Mattout et al. 2006). Two main lamin classes have been defined, type A and type B, on the basis of their protein structure, biochemical properties, expression patterns and behaviour during mitosis (for a review see Broers et al. 2006). The B-type lamins are expressed in every cell, whereas expression of A-type lamins is developmentally regulated. Lamins are involved in maintaining the stability and shape of the nucleus, chromatin organization, gene expression, DNA replication and transcription, nuclear transport, cell-cycle regulation, apoptosis, cell development and differentiation, nuclear anchoring and migration, and centrosome positioning (Gruenbaum et al. 2005; Broers et al. 2006). Furthermore, lamins play key roles in vertebrate development, especially that of mesodermal/mesenchymal derivatives (Csoka et al. 2004; Foster et al. 2007).

Recently, it has been demonstrated that mutations in the genes coding for A-type lamins, lamin A-related proteins, or ZMPSTE24 (a metalloproteinase implicated in the post-translational processing of prelamin A), cause a variety of heritable human diseases, known collectively as laminopathies (Mounkes et al. 2003; Navarro et al. 2005; Somech et al. 2005; Broers et al. 2006; Jacob & Garg, 2006; Worman & Bonne, 2007). These diseases are clinically heterogeneous, extending from cardiac and skeletal muscle disease or lipodystrophy to premature ageing phenotypes (Cadinanos et al. 2005; Liu et al. 2005; Shackleton et al. 2005; Smith et al. 2005; Navarro et al. 2006; Ramirez et al. 2006). Typically, some laminopathies, such as mandibuloacral dysplasia

Correspondence
Juan M. Cobo, Instituto Asturiano de Odontología, Cl Catedrático Jose M. Serrano, 8-10, 33006 OVIEDO, Spain. E: jcobo@odontológico.com

Accepted for publication *16 July 2008*

(Hoeffel et al. 2000) or Hutchinson–Gilford progeria syndrome (HGPS), have a craniofacial phenotype (Pollex & Hegele, 2004; Hennekam, 2006). Patients suffering HGPS show facial features that resemble aged persons, including abnormal mandible (micrognatia) associated with mandibuloacral dysplasia and osteolysis in the viscerocranium bones (Denecke et al. 2006; Hennekam, 2006), as well as aberrant odontogenesis with dental dysplasia and demineralization with multiple cavities (De Paula Rodrigues et al. 2002; Plasilova et al. 2004). On the other hand, mandibuloacral dysplasia is characterized by mandibular hypoplasia, delayed closure of cranial sutures, micrognatia, dental alterations and progeroid facies (Novelli et al. 2002; Simha & Garg, 2002; Agarwal et al. 2003; Shen et al. 2003; Simha et al. 2003; Afifi & El-Bassyouni 2005; Garg et al. 2005).

Mice models generated to analyse the genetic defects resulting in abnormal craniofacial development have provided valuable information to our understanding of these malformations (see Verdyck et al. 2006). Thus, mice strains carrying mutations in the *Zmpste24* gene are regarded as a model to study laminopathies. They develop accelerated ageing (Pendas et al. 2002; Varela et al. 2005; Espada et al. 2008) and a cranial phenotype consisting of defects of the posterior portion of the zygomatic arch, striking microcephalia and reduction of the interdigitations in cranial sutures (Bergo et al. 2002; Fong et al. 2006). Nevertheless, the impact of these mutations in the skull and teeth has not been evaluated in detail. Here we analysed in detail the cranium, with special reference to the mandible, of adult *Zmpste24* deficient mice using micro computed tomography (μCT). Furthermore, using simple radiology, μCT, μCT-differential densitometry, scanning electron microscopy and structural techniques, the morphology and structure of the tooth in these mice were analysed. Our results demonstrate that *Zmpste24*$^{-/-}$ mice show microcephalia with mandibular and dental dysplasia.

Material and methods

Animals

Adult male mice, aged 4 months, carrying a targeted mutation of the *Zmpste24* gene that causes an absence of the gene product (Pendás et al. 2002), were obtained from the colony of the Departamento de Bioquímica y Biología Molecular, Universidad de Oviedo, Spain. Wild-type ($n = 6$) and homozygous *Zmpste24*$^{-/-}$ ($n = 6$) mice were included in this study. The animals were deeply anaesthetized with chloral hydrate (350 mg kg^{-1}, i.p.), weighed and killed by decapitation. Animal housing and all experiments were performed according to the animal care guidelines of the European Community Council (86/609/EE).

Radiological and μCT studies

The preliminary radiographic study was performed in anaesthetized living animals using a human intraoral radiographic system (Siemens Heliodent 60, Germany) and Kodak DF-50 radiographic films. After the animals had been killed, the heads of wild-type and *Zmpste24*$^{-/-}$ mice were isolated, cleaned of skin and loose musculature, and the cranial organs, i.e. tongue and eyes, were removed. Thereafter, the skulls were examined with a MicroCT Skyscan 1172 system (Skyscan N.V., Aartselaar, Belgium). The images of both groups of animals were generated at identical threshold, and were obtained at a voltage of 70 kV, a current of 140 μA, using an aluminium filter of 1.0 mm thickness, at an isotropic resolution of 17.5 μm. The rotational angle was of 185° with increasing values of 90°. The voxel size selected was 17.5 μm. The images were reconstructed using the modified algorithm of Feldkamp et al. (1984) and the binary images were segmented using an umbralization of local adaptation (Liu & Sasov, 2005). Furthermore, using the specific software of the system, a differential densitometric study of the mandible and the lower incisor was carried out.

Craniometric mesurements

Eleven measurements for the cranium and nine for the mandible were evaluated. All these measurements were distances between recognizable landmarks on digitized images of the normae dorsalis, basalis and lateralis dextra and lateralis sinistra of the skull. The craniometric mandible measurements were made on the articulated bone, whereas the other morphological details, i.e. angles, were made on isolated bone. The measurements taken were based on other studies carried out in mice showing skull phenotypes caused by gene mutation (see Olafsdottir et al. 2007), and were homologous to those used for standard orthodontic cephalometry in humans (Burkhardt et al. 2003). Furthermore, the cranial and oral volumes were calculated automatically by the μCT system. In the skulls of both groups of animals, the following parameters were measured (Fig. 1):

Craniometric measurements:

1 Cranial length: measured between the internasal (top of the nose) and the occipital (the most distal point of the occipital bone) points.

2 Inter-orbitary length: measured between right and left infraorbital foramina.

3 Inter-nasal distance: measured between both nasal lateral points.

4 Inter-zygomatic distance: measured between both zygion points.

5 Bi-temporal distance: measured in the more distant point of the jugal process off squamosal with respect to the sagittal plane.

6 Sagittal cranial distance: measured between the occipital and the naso-maxillary point.

7 Posterior cranial height: measured between the tympanic and the parietal point.

8 Anterior cranial height: measured between the upper incisor and the prosthion points.

9 Upper incisor height: measured between the upper incisor–alveolar bone and upper incisor edge.

10 Palatine length: measured between the posterior nasal spine and the inter-dental point.

11 Inter-molar maxillary distance: measured between the left and right molar fosses.

Mandible measurements:

1 Posterior mandible height: measured between the gonion and condylion points.

2 Condylar axis (length of the ascending ramus): measured between the condylion and antegonion points.

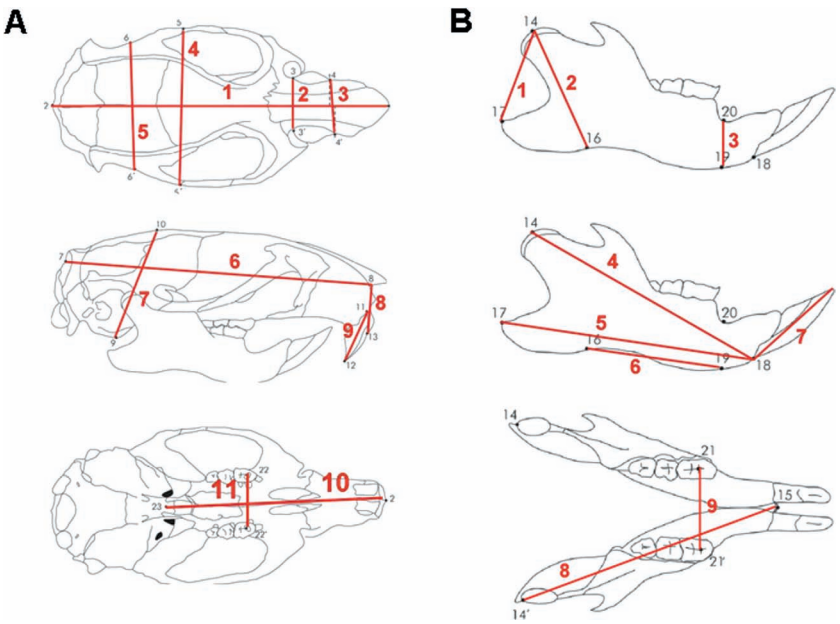

Fig. 1 Craniometric (A) and mandible (B) measurements carried out in wild-type and *Zmpste24*$^{-/-}$ mice. Red lines and red numbers indicate each measurement. Numbers in black correspond to landmark points. Drawings were designed from radiographic images. (A) 1, inter-nasal point; 2, occipital point; 3–3′, orbitary points (right and left infraorbital foramina); 4–4′, nasal points; 5–5′, zygomatic points; 6–6′, (jugal process off squamosal); 7, occipital point; 8, naso-maxillary point; 9, tympanic point; 10, parietal point; 11, superior incisor–alveolar point; 12, superior incisor point; 13, prostion; 22–22′, fosse of the maxillary central molar; 23, posterior nasal spine; 24, maxillary inter-dental point. (B) 14–14′, condylion point; 15, mandible inter-dental point; 16, antegonion; 17, gonion; 18, inferior incisor–alveolar point; 19, menton; 20, mandible alveolar (or diastema) point; 21, inferior incisor point.

3 Anterior mandible height: measured between the menton and the mandibular alveolar (or diastema) points.
4 Effective mandible length: measured between the lower alveolar incisor (infradentale) and the condylion points.
5 Mandible plain: measured between the gonion and the lower incisor–alveolar bone.
6 Mandible axis: measured between the antegonium and menton points.
7 Inferior incisor height: measured between the lower incisor–alveolar bone and the lower edge.
8 Hemi-mandible length: measured between the condylion and inter-dental points.
9 Inter-molar mandible length: measured between the left and right molar fosses between the right and left molar fosses.
All results are expressed as mean ± standard error of the mean of the wild-type and mutant animals. Statistical comparisons were carried out using the non-parametric Mann–Whitney *U*-test. A value of $P < 0.05$ was considered as significant.

Scanning electron microscopy

The incisors (one per animal) and molars attached to the maxillary bone and the mandible were processed for scanning electron microscopy after μCT study. The pieces were washed in 5% neutral Extran (Merck, Darmstadt, Germany) to remove debris. The pieces were then rinsed in 0.1 M Sörensen phosphate buffer (pH 7.2), dehydrated in a graded series of alcohol, submitted to critical-point drying in a Balzers CPD 030, sputter coated with gold in a Balzers BAL-TEC SCD 050, and examined under a Cambridge Stereoscan 240 scanning electron microscope at an accelerating voltage of 20 kV.

Structural study of the lower incisors

The lower incisors (one per animal) were removed from the mandible, and decalcified with EDTA in 0.1 M phosphate-buffered saline (pH = 7.2). Thereafter, the pieces were rinsed in the same buffer as above, dehydrated and routinely embedded in paraffin. Longitudinal sections were obtained, mounted on microscope slides, and processed for haematoxylin-eosin staining.

Results

Mice carrying a mutation in the *Zmpste24* gene when studied at 4 months of age showed severe growth retardation and morphological signs consistent with premature ageing; the skeletal muscles and the skin displayed the typical alterations that characterize the phenotype of these animals (see Pendas et al. 2002). Nevertheless, the present study was focused on the skull and teeth.

μCT study

The observation of the skull surface shows that the osseous relieves were less marked and the indentations of the sutures between cranial bones were morphologically reduced in *Zmpste24*-deficient animals in relation to their wild-type littermates, affecting primarily the coronal (fronto-parietal) and the lambdoidal (parieto-occipital) sutures (Figs 2 and 3). In one wild-type mouse (1/6) and in one *Zmpste24*-deficient mouse (1/6), a defect in the zygomatic arch was observed by μCT (Figs 2 and 3, arrows). The images were consistent with the absence of a small segment in this structure, and it was localized at the posterior portion of the zygomatic arch in the wild-type mouse, whereas in the *Zmpste24*$^{-/-}$ mice the defect involved the anterior segment. It must be emphasized that the zygomatic arch of the remaining animals included in the study was normal, and that this kind of defect was not found in standard radiographies or in conventional CT (data not shown). Therefore, we conclude

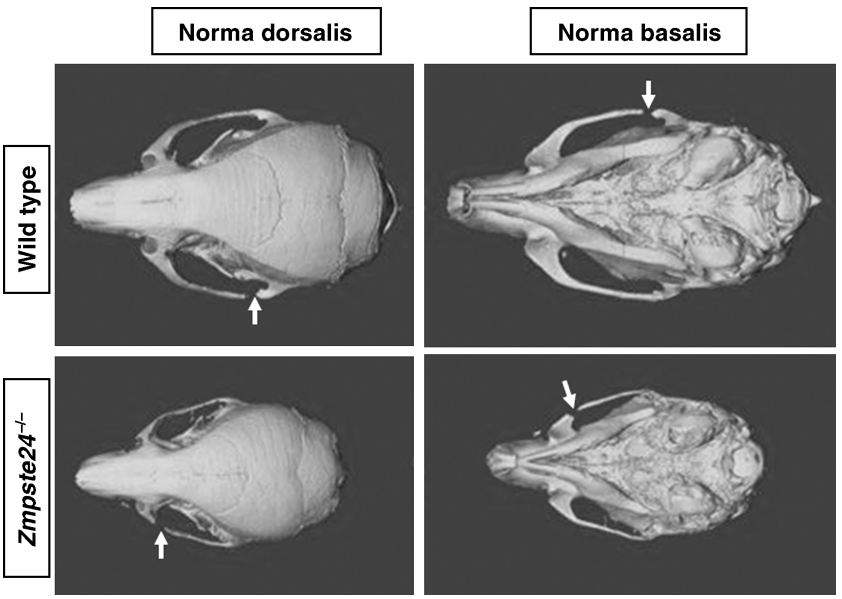

Fig. 2 μCT scans showing the cranial morphology of wild-type and *Zmpste24*$^{-/-}$ mice, as observed dorsally and basally. Arrows indicate absence of small fragments in the zygomatic arch in both wild-type and mutant animals. Another remarkable fact observed in the *Zmpste24*$^{-/-}$ mice was a reduction in the indentations of the cranial sutures. Enlargement of the figures from wild-type and *Zmpste24*$^{-/-}$ mice was identical to illustrate the reduction of the skull in mutated animals. Scale bar = 1 cm.

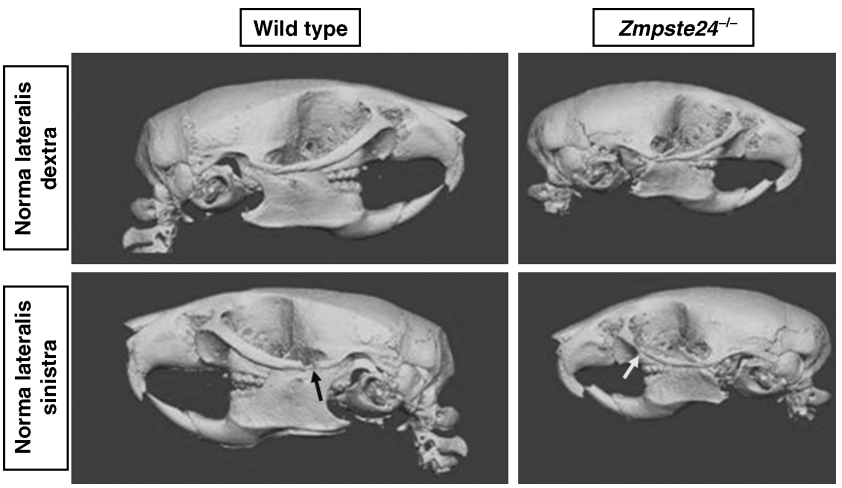

Fig. 3 μCT scans showing the cranial morphology of wild-type and *Zmpste24*$^{-/-}$ mice (lateral view). Arrows indicate absence of small segments in the zygomatic arch in both wild-type and mutant animals. Enlargement of the figures from wild-type and *Zmpste24*$^{-/-}$ mice was identical to illustrate the reduction of the skull in mutated animals. Scale bar = 1 cm.

that these lesions in the zygomatic arch are probably due to the manipulative procedures in cleaning the cranium for μCT study rather than to *Zmpste24*-deficiency.

Craniometric analysis

The skull of the mutant mice was smaller than that of their wild-type counterparts, and the measurements made on the cranium of *Zmpste24*$^{-/-}$ mice demonstrate that they are microcephalic: all the distances measured were reduced with respect to the wild-type animals, although not all the measured distances were statistically reduced (Table 1). Furthermore, the total skull volume in wild-type animals was 218.03 ± 22.18 mm^3 compared with 161.38 ± 23.06 mm^3 in *Zmpste24*$^{-/-}$ mice. This equates to a reduction in the cranial volume of the mutated mice of about 26%. Oral volumes were 97.33 ± 12.16 mm^3 in wild-type mice and 69.46 ± 12.16 mm^3 in those carrying the *Zmpste24* mutation, a reduction of about 25%, slightly less marked than that of the whole skull. Both reductions in mutated animals were statistically significant.

Mandible measurements

As for the cranium, most of the measurements taken on the mandible were reduced in *Zmpste24*$^{-/-}$ mice with respect to their wild-type littermates, with the exception of intermolar diameter (Table 1). The largest decreases were observed in the vertical and in the antero-posterior measurements. These variations are presumably related to the reduced size of both condyle and gonion (Fig. 3). Furthermore, the osseous relieves of the mandible were less marked in mutant mice than in their wild-type littermates (Fig. 4). In addition, there were radiographic signs of bone defect,

Table 1 Results of the craniometric and mandible measurements in wild-type and *Zmpste24*$^{-/-}$ mice corresponding to the red lines indicated in Fig. 1A,B. Results are values of mean ± SEM, and are expressed in mm

	WT	*Zmpste24*$^{-/-}$ mice	Variation (%)
Cranial measurements			
Line 1: CL	22.64 ± 0.26	20.07 ± 0.33*	–11
Line 2: Inter-orbitary L	4.12 ± 0.08	3.88 ± 0.15	–6
Line 3: Internasal D	3.79 ± 0.06	3.50 ± 0.09*	–8
Line 4: Interzygomatic D	12.01 ± 0.21	10.80 ± 0.16*	–10
Line 5: Bi-temporal D	10.57 ± 0,13	10.00 ± 0.16	–5
Line 6: Sagittal CD	21.07 ± 0.33	18.58 ± 0.43*	–12
Line 7: Posterior CH	10.25 ± 0.16	8.94 ± 0.47*	–13
Line 8: Anterior CH	2.71 ± 0.07	2.57 ± 0.19	–5
Line 9: Upper incisor H	3.99 ± 0.18	3.66 ± 0.12	–8
Line 10: Palatine L	13.98 ± 0.09	12.80 ± 0.37	–8
Line 11: Inter-molar maxillary	4.24 ± 0.06	4.09 ± 0.27*	–4
Mandible measurements			
Line 1: Posterior MH	4.04 ± 0.06	3.04 ± 0.26*	–25
Line 2: Condyloid axis	5.19 ± 0.09	3.63 ± 0.28*	–30
Line 3: Anterior MH	2.08 ± 0.08	2.07 ± 0.10	0
Line 4: Effective ML	11.19 ± 0.21	8.24 ± 0.37*	–26
Line 5: M plain	10.44 ± 0.65	7.97 ± 0.34*	–24
Line 6: M axis	5.46 ± 0.45	3.59 ± 0.31*	–34
Line 7: Inferior incisor axis	4.38 ± 0.09	4.05 ± 0.26	–8
Line 8: Hemi-ML	13.83 ± 0.96	13.62 ± 0.56	–2
Line 9: Inter-molar ML	4.85 ± 0.58	5.18 ± 0.47	+6

C = cranial; M = mandible.
D = distance; H = height; L = length.
*$P < 0.05$.

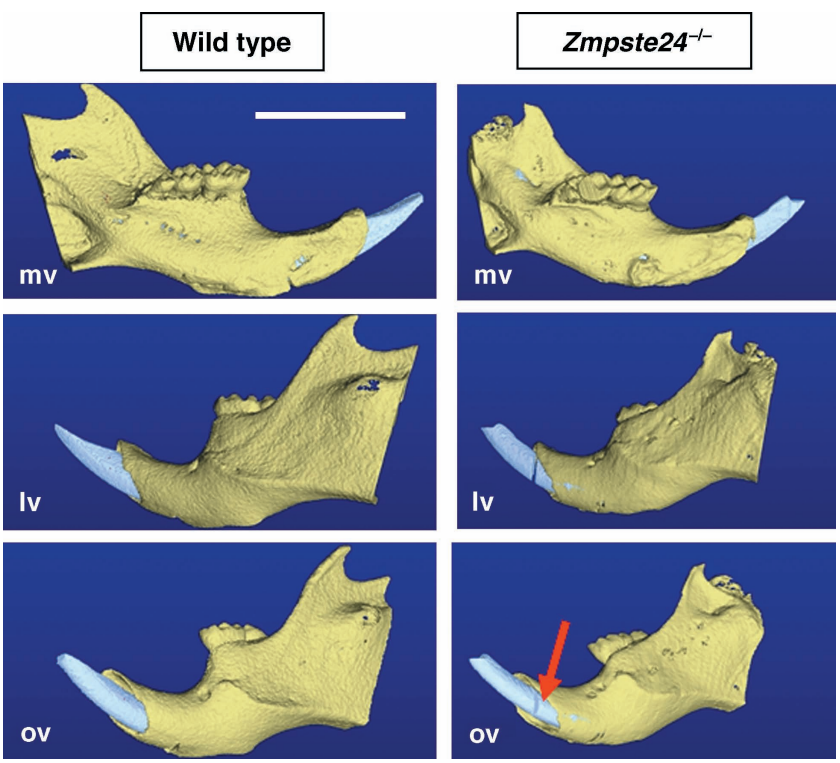

Fig. 4 µCT scans of the mandible isolated in wild-type and *Zmpste24*$^{-/-}$ mice, as observed medially (mv), laterally (lv) and obliquely (ov). The osseous relieves were less marked in the mutant animals than in controls, and the gonion, condylar process and coronoid process were also smaller. The mutant animals showed an apparent bone resorption of the alveolar bone (arrow). Scale bar = 5 mm.

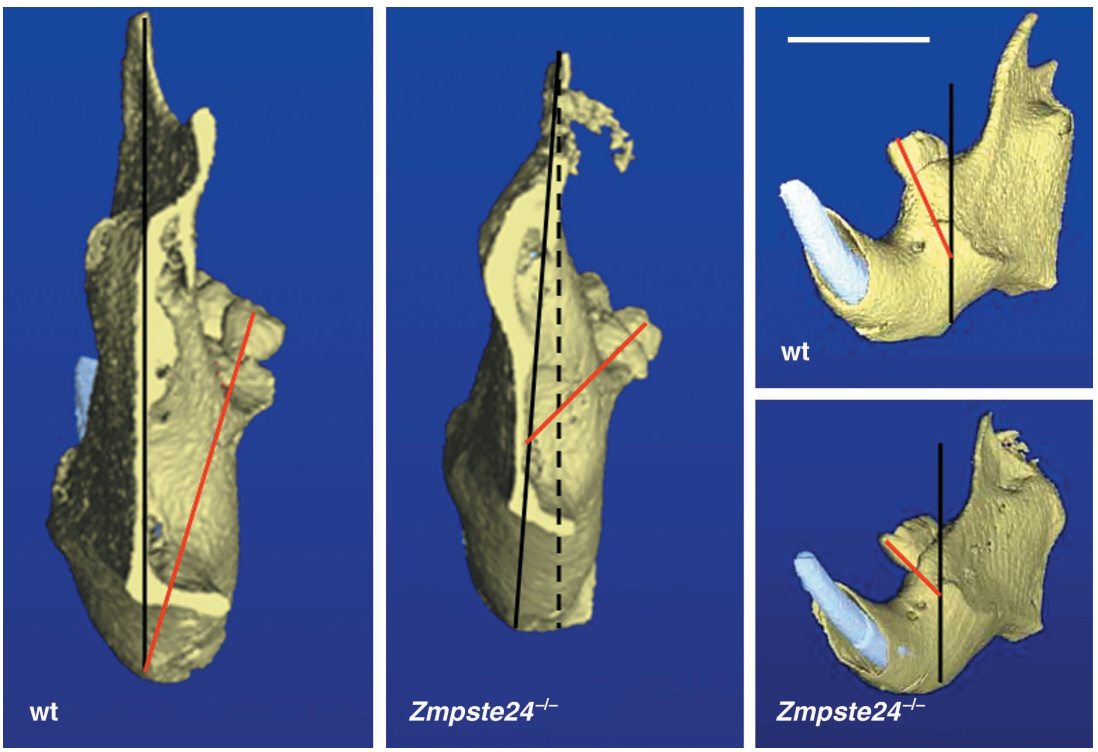

Fig. 5 μCT scans of the isolated mandible in wild-type (wt) and *Zmpste24*-deficient mice (*Zmpste24*$^{-/-}$) showing the implantation of the lower molars in the mandible. In both dorsal and oblique views the angle formed between the axis of third molar (red lines in large vertical figures) with respect to the posterior border of the mandible (or a vertical line: discontinuous line) and a tangent to the posterior border of the third molar (black lines) was wider in mutant animals than in wild-type ones. Scale bar = 5 mm.

presumably due to bone resorption, in the deficient mice especially affecting the medial part of the mandible at the level of the lower incisors implantation [Figs 4 (arrow) and 5]. Taken together, the results of skull measurements in *Zmpste24*$^{-/-}$ mice show that it is short and straight, and the mandible is short and flattened when compared with control littermates. The implantation of molars in the mandible also differed between the two groups of animals. In fact, the mean value of the angle formed between the vertical–posterior border of the mandible and the axis of the third molar was about $30 \pm 4°$ in wild-type animals, whereas in mutants this was $45 \pm 6°$ with respect to the posterior border of the mandible, and 35–40° with respect to the vertical. In external–oblique views of the mandible, the axis of the first molar forms an angle of 35° with a vertical line tangent to the posterior border of the third molar in control mice, while this angle reaches 45° in *Zmpste24*$^{-/-}$ mice (Fig. 5).

Size, shape and morphology of the teeth

During μCT study of the cranium we regularly observed that the incisors of the mutant mice showed anomalies in both implantation and morphology. Using simple radiology in lateral projections, it was observed that the upper incisor in *Zmpste24*-deficient animals had a curvature-radius smaller than in wild-type mice (Fig. 6), but no other morphological variations were detected. Nevertheless, the lower incisors clearly differed between the two groups of animals. The crown of the lower incisor in mutants was cylindrical rather than triangle-pyramidal, and the incisal edge was rounded, not cutting, and showed a transverse fissure (Fig. 6). The morphology of the upper molars in mutants was consistent with normality whereas the lower molars showed an evident reduction of the cusps, especially the lingual cusps (Fig. 6). Using μCT-densitometric techniques, we also studied the localization of the lower incisor within the mandible. The teeth of mutant animals were shorter, more curved and thicker than in controls; another important feature was that the retromolar segment of the teeth (i.e. placed dorsal to a line between the second molar and the gonion) was proportionally greater in *Zmpste24*$^{-/-}$ mice than in wild-type animals, as observed in images of differential densitometry. In addition, the pulpal cavity was very small and circumscribed to the posterior tip of the incisor in *Zmpste24* deficient mice while in wild-type animals, it occupied approximately the posterior half of the teeth (Fig. 7).

Structure of the lower incisor

Finally, we analysed the impact of the *Zmpste24* mutation on the structure of the lower incisor. The tooth was sampled

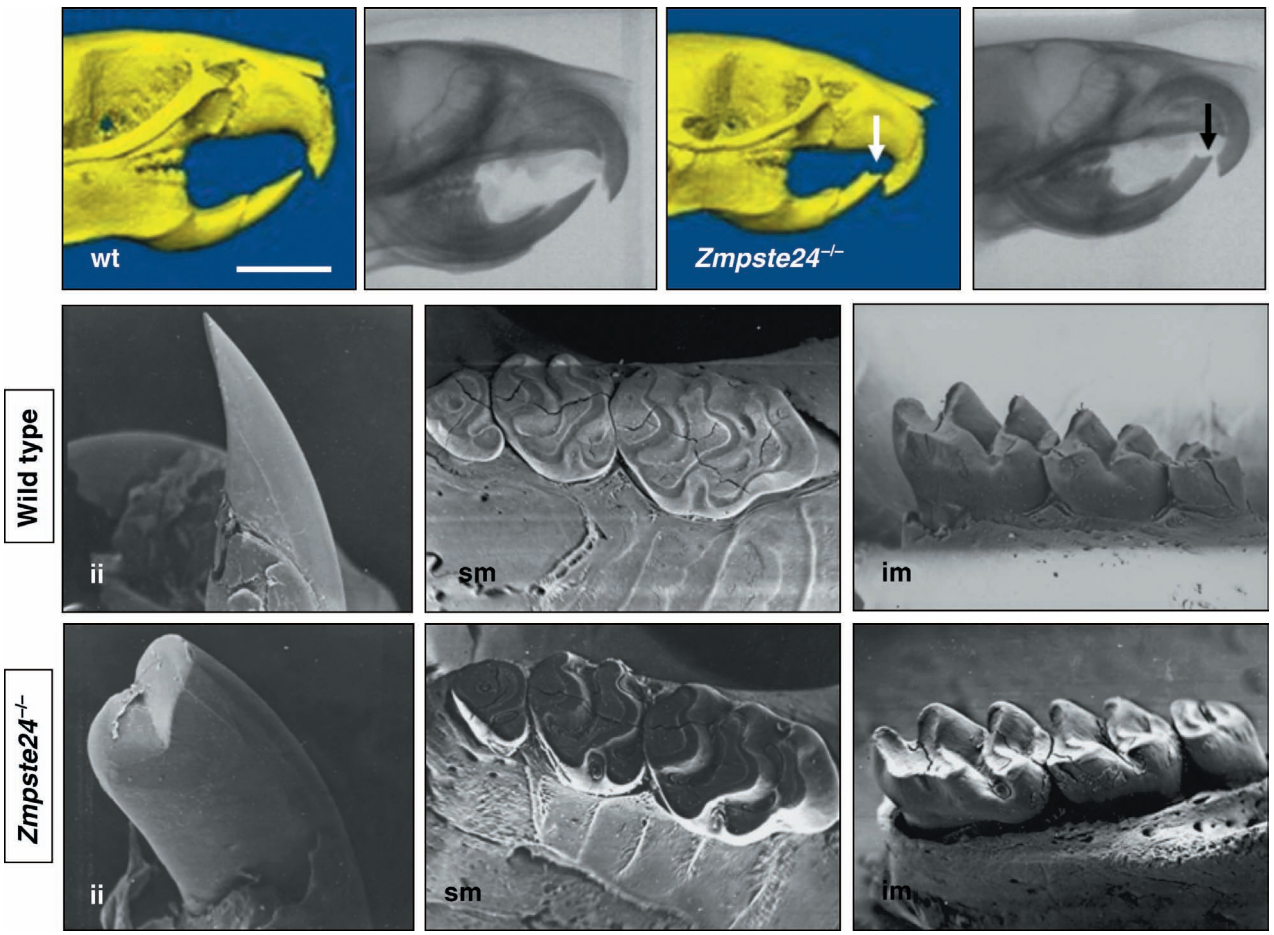

Fig. 6 Abnormal morphology of the lower incisor (arrows) in 4-month-old *Zmpste24*$^{-/-}$ mice as observed in μCT and simple radiology. In contrast to the triangular morphology of the lower incisor of wild-type (wt) mice, those from *Zmpste24*$^{-/-}$ animals were cylindrical and showed a transverse fissure at the incisal edge. The only variation observed in the upper incisor (ui) of *Zmpste24*$^{-/-}$ mice was an increase of the curvature without external morphological variation. Scanning electron microscopy (SEM) analysis of the crown surface of the lower incisors (li) in wild-type and mutant mice confirmed the abnormal morphology of this tooth in mutant mice and the occurrence of a transverse fissure at the free border. The upper molars (um) were almost identical in both groups of animals, whereas the lower molars (lm) of *Zmpste24*-deficient mice showed a reduction of the cusps in comparison with controls. Scale bar for μCT and simple radiology images = 5 mm; original magnification for SEM images: 15× for upper incisor, and 22× for lower incisor; 30× for molars.

at three different segments: extra-alveolar, the zone of the alveolar implantation and the inframolar; the most posterior segment was not analysed. As expected, histological examination of the decalcified crown showed exclusively the occurrence of enamel, but the morphology differed in the two groups of animals, having a triangular shape in longitudinal sections in wild-type mice (Fig. 8A) and almost cylindrical with a V-shaped incisal edge in the *Zmpste24*-null mice (Fig. 8B,C). The tooth structure in the transitional zone demonstrates the presence of pulpal cavity in the control animals, whereas it was completely absent in the mutants (Fig. 8D,E). The posterior segment examined showed a well-developed pulpal cavity (Fig. 8F,G) which was larger in the control than in mutant animals. This cellular space was connected with the mandibular bone and the attachment was irregular in the mutant animals. Detailed examination of the tooth structure revealed that the ameloblasts in the *Zmpste24*-deficient animals were smaller and apparently atrophic as compared with controls (Fig. 8H,I).

Discussion

The development of the vertebrate head results from complex multidirectional interactions among the three embryonic layers, influenced by neural crest cells. In recent years, critical information has been added on the molecular mechanisms that are crucial for the patterning and formation of craniofacial structures. The genes that control their development include those coding for growth factors, transcription factors, and proteins involved in cell proliferation and migration (for reviews see Helms et al. 2005; Chai & Maxson, 2006; Sauka-Spengler & Bronner-Fraser, 2006). This knowledge

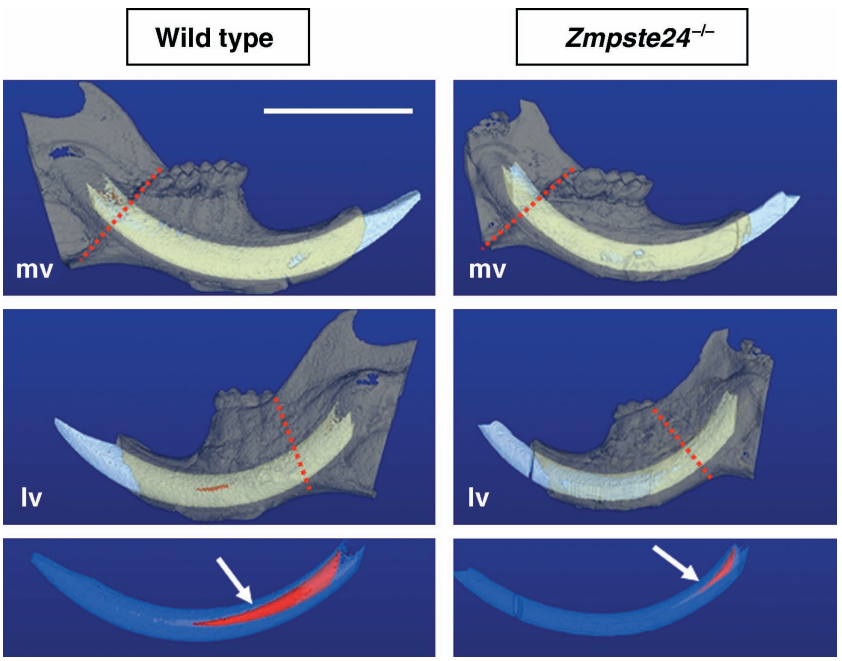

Fig. 7 Differential μCT of the mandible and the lower incisor in wild-type (wt) and *Zmpste24*-deficient mice (*Zmpste24*$^{-/-}$) as observed in medial (mv) and lateral (lv) views. The lower molar was normally implanted within the mandible, although the segment placed in the retromolar space (segment of the mandible localized dorsally to a line between the third molar and the ategonion) was greater in mutant animals than in controls. By contrast, the pulpal cavity (red images indicated by arrows) was severely reduced in *Zmpste24*-deficient animals. Scale bar = 5 mm.

is critical to a better understanding of the mechanisms involved in craniofacial malformations (Wilkie & Morriss-Kay, 2001; Francis-West et al. 2003). According to van der Meulen et al. (1983) and Vermeij-Keers et al. (1983), two main categories of craniofacial malformations can be considered: those involving skull and neural elements of the head (brain, eyes) and those specific to the face and cranium, i.e. the musculoskeletal craniofacial dysplasias. These latter malformations involve defective differentiation to the neurectoderm and the mesenchyme into bone centres, cartilage and muscles. In recent years, different animal models, especially mouse (Thyagarajan et al. 2003) and zebrafish (Yelick & Schilling, 2002), carrying mutations which result in loss-of-function of proteins assumed to be essential in head building have provided functional insights into the genes that are required for normal craniofacial development.

Abnormal morphology of the cranium, especially of the facial bones, is a characteristic of some laminopathies including progeroid syndromes such as HGPS (Pollex & Hegele, 2004; Hennekam, 2006), or rare heritable diseases such as mandibuloacral dysplasia (Novelli et al. 2002; Simha & Garg, 2002; Agarwal et al. 2003; Shen et al. 2003; Simha et al. 2003; Afifi & El-Bassyouni, 2005; Garg et al. 2005). Two genetic loci are known for HGPS and mandibuloacral dysplasia: *LMNA*, encoding nuclear lamin A/C, and *ZMPSTE24* (*FACE1*) encoding a membrane-bound metalloproteinase involved in post-translational proteolytic cleavage of carboxy-terminal residues of prelamin A to form mature lamin A (for references see Cadinanos et al. 2005). In both cases, the consequence of the mutations is an abnormally formed lamin A, which accumulates in the cell nucleus and is responsible for nuclear damage and disease (Worman & Courvalin, 2004; Scaffidi & Misteli, 2006).

The present study was designed to analyse the impact of *Zmpste24* deficiency in the skull and teeth of adult mice. Previous studies from our group (Pendas et al. 2002; Varela et al. 2005) and others (Bergo et al. 2002) have partially characterized the phenotype in two different strains of *Zmpste24* mutant mice. The whole aspect of the cranium of *Zmpste24*-deficient mice accurately studied with simple radiology and μCT displayed features of reduced growth rate with respect to the control littermates, based on maxillary vector growth (see Diemunsch et al. 2007), which has an anterior–superior direction in control animals whereas is flattened (more horizontal) in the mutants (F.d.C. et al. unpublished data). The craniometric study that we have conducted demonstrates that *Zmpste24*$^{-/-}$ mice show microcephalia associated with mandibular and dental dysplasia, but not micrognatia, a typical facial dismorphya in HGPS (Pollex & Hegele, 2004; Hennekam, 2006) and mandibuloacral dysplasia (Novelli et al. 2002; Agarwal et al. 2003; Shen et al. 2003; Afifi & El-Bassyouni 2005; Garg et al. 2005). Several alterations in the skeletal system, including the skull, of *Zmpste24*-deficient mice have been described by Bergo et al. (2002) and Fong et al. (2006). Nevertheless, we must emphasize that our results only partially agree with those reported by these authors. Thus, we have also observed a decrease in indentations in the skull sutures present in mutant animals, but we have failed to observe the micrognatia reported by them in *Zmpste24*$^{-/-}$ mice (Bergo et al. 2002). By contrast, we have detected a whole microcephalia, which also involves the mandible. Bergo et al. have also

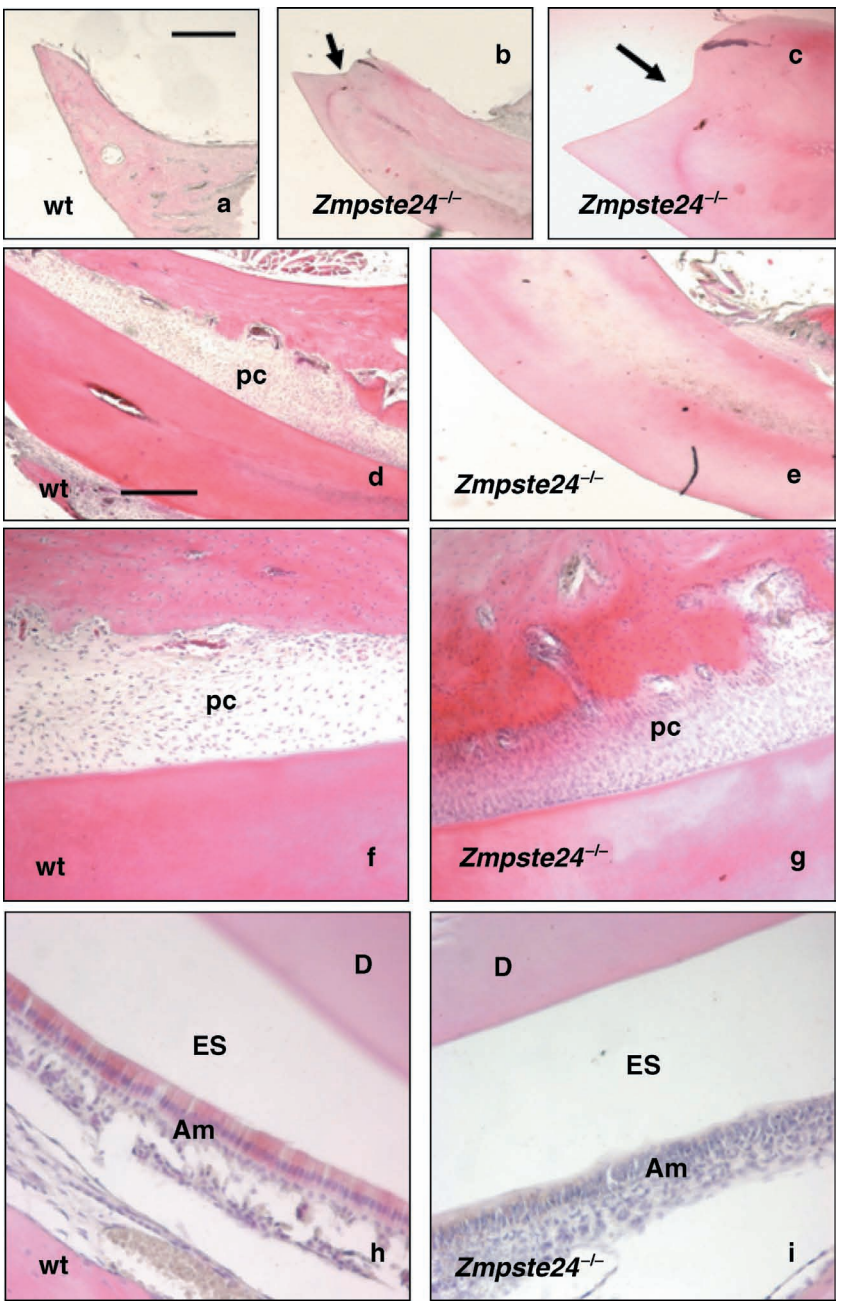

Fig. 8 Structure of the lower incisor in wild-type (wt) and *Zmpste24*-deficient mice (*Zmpste24*$^{-/-}$) as observed in longitudinal sections stained with H&E. In wild-type animals (a) the section was triangular in shape, whereas in the mutant animals it was cylindrical and showed a transverse fissure at the incisal edge (arrows in b and c). At the level of the alveolar border, a small pulpa cavity was observed in control mice (d) while it was absent in the mutant mice (e); the pulpal cavity was also greater in the inframolar segment of the inferior incisor in wild-type animals (f and g). The dental layers were well arranged in both groups of animals but the ameloblasts were less differentiated in the mutant mice. D, dentin; ES, enamel space; Am, ameloblast layer; pc, pulpal cavity. Scale bar = 3 mm for a,c; 0.8 mm for c; 85 mm for d,e; 50 mm for f,g; 20 mm for h,i.

reported that the mandible from mutant mice was normal in size and shape, at least in 18-day-old animals, suggesting that micrognatia in adult animals is secondary to zygomatic arch fractures. However, in our mutant mice, we have found a considerable reduction in mandible size, especially affecting the gonion, condyloid process and coronoid process. An additional feature invariably observed by Bergo et al. (2002) and Fong et al. (2006) was the presence of defects of the zygomatic arch in *Zmpste24*-deficient mice. We observed this defect in a single (1/6) mutant animal, but also in one wild-type mouse (1/6), the other animals analysed having a normal zygomatic arch. This lesion was never found with simple radiology or conventional scanning either in wild-type or in *Zmpste24*-deficient mice, thus suggesting that it is due to manipulative procedures in cleaning of the skulls for μCT analysis rather than to the mutation itself.

In addition to the skull anomalies, we also observed abnormal morphology, implantation and structure of the teeth, especially the lower incisor. Mice deficient in *Zmpste24* display morphological and structural changes in the lower incisor that are consistent with dental dysplasia; conversely, the maxillary incisors were apparently normal. The mandible incisor characteristically showed an abnormal morphology at the incisal edge, the dentin layer was thicker than in

wild-type littermates, and the pulpar chamber was almost non-existent. At the structural level the cellular layer of the ameloblasts was disarranged, but these alterations need to be analysed in future studies using more sensitive techniques. An identical μCT imaging of the lower incisor was shown by Fong et al. (2006), although these authors do not describe this anomaly. Also, there was a reduction of the cusps in the mandible molar. Nevertheless, it is difficult to assimilate these lesions with the dental aberrations described in human HGPS and mandibuloacral dysplasia (De Paula Rodrigues et al. 2002: Plasilova et al. 2004).

In conclusion, the abnormalities described here support the use of *Zmpste24*-deficient mice as a model to investigate the craniofacial and teeth malformations characteristic of lamin-related pathologies, and might contribute to a better understanding of the molecular events underlying these diseases. The structural basis of most of the morphological changes described here remains to be analysed, and experiments are in progress in our laboratories to elucidate these aspects. Moreover, in the absence of experimental data demonstrating neuro-visceral damage associated with the skull changes, our data demonstrate that *Zmpste24*-deficient mice develop an equivalent to the human musculoskeletal craniofacial dysplasias (van der Meulen et al. 1983; Vermeij-Keers et al. 1983).

Acknowledgments

This work was supported by grants from the Ministerio de Educación y Ciencia-Spain, Fundación La Caixa and Fundación M. Botín, The Instituto Universitario de Oncología is supported by Obra Social Cajastur-Asturias, Spain. The radiological study was supported by Instituto Asturiano de Odontología. We thank Professor J. C. de Vicente for help with statistical analysis.

References

Afifi HH, El-Bassyouni HT (2005) Mandibuloacral dysplasia: a report of two Egyptian cases. *Genet Couns* **16**, 353–362.

Agarwal AK, Fryns JP, Auchus RJ, Garg A (2003) Zinc metalloproteinase, ZMPSTE24, is mutated in mandibuloacral dysplasia. *Hum Mol Genet* **12**, 1995–2001.

Bergo MO, Gavino G, Ross J, et al. (2002) *Zmpste24* deficiency in mice causes spontaneous bone fractures, muscle weakness, and a prelamin A processing defect. *Proc Natl Acad Sci USA* **99**, 13049–13054.

Broers JLV, Ramaekers FCS, Bonne G, Ben Yaou R, Hutchison CJ (2006) Nuclear lamins: laminopathies and their role in premature aging. *Physiol Rev* **86**, 967–1008.

Burkhardt DR, McNamara JA Jr, Baccetti T (2003) Maxillary molar distalization or mandibular enhancement: a cephalometric comparison of comprehensive arthodontic treatment including the pendulum and the Herbst appliances. *Am J Orthod Dentofacial Orthop* **123**, 108–116.

Cadinanos J, Varela I, Lopez-Otin C, Freije JM (2005) From immature lamin to premature aging: molecular pathways and therapeutic opportunities. *Cell Cycle* **4**, 1732–1735.

Chai Y, Maxson RE Jr. (2006) Recent advances in craniofacial morphogenesis. *Dev Dyn* **235**, 2353–2375.

Csoka AB, English SB, Simkevich CP, et al. (2004) Genome-scale expression profiling of Hutchinson–Gilford progeria syndrome reveals widespread transcriptional misregulation leading to mesodermal/mesenchymal defects and accelerated atherosclerosis. *Aging Cell* **3**, 235–243.

De Paula Rodrigues GH, das Eiras Talega I, Duque G, Dias Neto VS (2002) Severe bone changes in a case of Hutchinson–Gilford progeria. *Ann Genet* **45**, 151–155.

Denecke J, Brune T, Feldhaus T, et al. (2006) A homozygous ZMPSTE24 null mutation in combination with a heterozygous mutation in the LMNA gene causes Hutchinson–Gilford progeria syndrome (HGPS): insights into the pathophysiology of HGPS. *Hum Mutat* **27**, 524–531.

Diemunsch C, Faure F, Trunde F, et al. (2007) Three-dimensional modeling system for unilateral mandibular bone distraction: a clinical case. *Comput Aided Surg* **12**, 262–269.

Espada, J, Varela I, Flores I, et al. (2008) Nuclear envelope defects cause stem cell dysfunction in premature-aging mice. *J Cell Biol* **181**, 27–35.

Feldkamp LA, Davis LC, Crees JW. (1984) Practical cone-beam algorithm. *J Opt Soc Am* **1**, 612–619.

Fong LG, Ng JK, Lammerding J, et al. (2006) Prelamin A and lamin A appear to be dispensable in the nuclear lamina. *J Clin Invest* **116**, 743–752.

Foster HA, Stokes P, Forsey K, Leese HJ, Bridger JM (2007) Lamins A and C are present in the nuclei of early porcine embryos, with lamin A being distributed in large intranuclear foci. *Chromosome Res* **15**, 163–174.

Francis-West PH, Robson L, Evans DJ (2003) Craniofacial development: the tissue and molecular interactions that control development of the head. *Adv Anat Embryol Cell Biol* **169**, III–VI, 1–138.

Garg A, Cogulu O, Ozkinay F, Onay H, Agarwal AK (2005) A novel homozygous Ala529Val LMNA mutation in Turkish patients with mandibuloacral dysplasia. *J Clin Endocrinol Metab* **90**, 5259–5264.

Gruenbaum Y, Margalit A, Goldman RD, Shumaker DK, Wilson KL (2005) The nuclear lamina comes of age. *Nat Rev Mol Cell Biol* **6**, 21–31.

Helms JA, Cordero D, Tapadia MD (2005) New insights into craniofacial morphogenesis. *Development* **132**, 851–861.

Hennekam RC (2006) Hutchinson–Gilford progeria syndrome: review of the phenotype. *Am J Med Genet* **140**, 2603–2624.

Hoeffel JC, Mainard L, Chastagner P, Hoeffel CC (2000) Mandibuloacral dysplasia. *Skeletal Radiol* **29**, 668–671.

Jacob KN, Garg A (2006) Laminopathies: multisystem dystrophy syndromes. *Mol Genet Metab* **87**, 289–302.

Liu B, Wang J, Chan KM, et al. (2005) Genomic instability in laminopathy-based premature aging. *Nat Med* **11**, 780–785.

Liu X, Sasov A (2005) Cluster reconstruction strategies for microCT and nanoCt scanners. In: *Proceedings of the Fully Three-Dimensional Image Reconstruction*. The Eight International Meeting in Radiology and Nuclear Medicine, Salt Lake City, Utah, pp. 215–218 (http://www.ucair.med.utah.edu/3D05).

Mattout A, Dechat T, Adam SA, et al. (2006) Nuclear lamins, diseases and aging. *Curr Opin Cell Biol* **18**, 335–341.

Mounkes L, Kozlov S, Burke B, Stewart CL (2003) The laminopathies: nuclear structure meets disease. *Curr Opin Genet Develop* **13**, 223–230.

Mounkes L, Stewart CL (2004) Structural organization and functions of the nucleus in development, aging and disease. *Curr Top Dev Biol* **61**, 191–228.

Navarro CL, Cadinanos J, De Sandre-Giovannoli A, et al. (2005) Loss of ZMPSTE24 (FACE-1) causes autosomal recessive restrictive

dermopathy and accumulation of Lamin A precursors. *Hum Mol Genet* **14**, 1503–1513.

Navarro CL, Cau P, Levy N (2006) Molecular bases of progeroid syndromes. *Hum Mol Genet* **15**, R151–R161.

Novelli G, Muchir A, Sangiuolo F, et al. (2002) Mandibuloacral dysplasia is caused by a mutation in LMNA-encoding lamin A/C. *Am J Hum Genet* **71**, 426–431.

Olafsdottir H, Darvann TA, Hermann NV, et al. (2007) Computacional Mouse atlases and their application to autosomic assessment of craneofacial dysmorphology caused by the Crouzon mutation *Fgfr2*^{C342Y}. *J Anat* **211**, 37–52.

Pendas AM, Zhou Z, Cadinanos J, et al. (2002) Defective prelamin A processing and muscular and adipocyte alterations in Zmpste24 metalloproteinase-deficient mice. *Nat Genet* **31**, 94–99.

Plasilova M, Chattopadhyay C, Pal P, et al. (2004) Homozygous missense mutation in the lamin A/C gene causes autosomal recessive Hutchinson–Gilford progeria syndrome. *J Med Genet* **41**, 609–614.

Pollex RL, Hegele RA (2004) Hutchinson–Gilford progeria syndrome. *Clin Genet* **66**, 375–381.

Ramirez CL, Cadinanos J, Varela I, Freije JM, Lopez-Otin C (2006) Human progeroid syndromes, aging and cancer: new genetic and epigenetic insights into old questions. *Cell Mol Life Sci* **64**, 155–170.

Sauka-Spengler T, Bronner-Fraser M (2006) Development and evolution of the migratory neural crest: a gene regulatory perspective. *Curr Opin Genet Dev* **16**, 360–366.

Scaffidi P, Misteli T (2006) Lamin A-dependent nuclear defects in human aging. *Science* **312**, 1059–1063.

Shackleton S, Smallwood DT, Clayton P, et al. (2005) Compound heterozygous ZMPSTE24 mutations reduce prelamin A processing and result in a severe progeroid phenotype. *J Med Genet* **42**, e36.

Shen JJ, Brown CA, Lupski JR, Potocki L (2003) Mandibuloacral dysplasia caused by homozygosity for the R527H mutation in lamin A/C. *J Med Genet* **40**, 854–857.

Simha V, Garg A (2002) Body fat distribution and metabolic derangements in patients with familial partial lipodystrophy associated with mandibuloacral dysplasia. *J Clin Endocrinol Metab* **87**, 776–785.

Simha V, Agarwal AK, Oral EA, Fryns JP, Garg A (2003) Genetic and phenotypic heterogeneity in patients with mandibuloacral dysplasia-associated lipodystrophy. *J Clin Endocrinol Metab* **88**, 2821–2824.

Smith ED, Kudlow BA, Frock RL, Kennedy BK (2005) A-type nuclear lamins, preogerias and other degenerative disorders. *Mech Ageing Dev* **126**, 447–460.

Somech R, Sharklal S, Amariglio N, Rechavi G, Simon AJ (2005) Nuclear envelopathies – Raising the nuclear veil. *Pediatric Res* **57**, 8R–15R.

Thyagarajan T, Totey S, Danton MJ, Kulkarni A (2003) Genetically altered mouse models: the good, the bad, and the ugly. *Crit Rev Oral Biol Med* **14**, 154–174.

van der Meulen JC, Mazzola R, Vermey-Keers C, Stricker M, Raphael B (1983) A morphogenetic classification of craniofacial malformations. *Plast Reconstr Surg* **71**, 560–572.

Varela I, Cadinanos J, Pendas AM, et al. (2005) Accelerated ageing in mice deficient in Zmpste24 protease is linked to p53 signalling activation. *Nature* **437**, 564–568.

Verdyck P, Wuyts W, Van Hul W (2006) Genetic defects in the development of the skull vault in humans and mice. *Crit Rev Eukaryot Gene Expr* **16**, 119–142.

Vermeij-Keers C, Mazzola RF, Van der Meulen JC, Strickler M (1983) Cerebro-craniofacial and craniofacial malformations: an embryological analysis. *Cleft Palate J* **20**, 128–145.

Wilkie AO, Morriss-Kay GM (2001) Genetics of craniofacial development and malformation. *Nat Rev Genet* **2**, 458–468.

Worman HJ, Bonne G (2007) Laminopathies: a wide spectrum of human diseases. *Exp Cell Res* **313**, 2121–2133.

Worman HJ, Courvalin JC (2004) How do mutations in lamins A and C cause disease? *J Clin Invest* **113**, 349–351.

Worman HJ, Courvalin J-C (2005) Nuclear envelope, nuclear lamina, and inherited disease. *Int Rev Cytol* **246**, 231–278.

Yelick PC, Schilling TF (2002) Molecular dissection of craniofacial development using zebrafish. *Crit Rev Oral Biol Med* **13**, 308–322.